INSTITUTE OF PHYSICS PUBLISHING INVERSE PROBLEMS

Inverse Problems **18** (2002) 559–573 PII: S0266-5611(02)28882-6

Estimation of optical absorption in anisotropic background

Jenni Heino[1] **and Erkki Somersalo**[2]

[1] Helsinki University of Technology, Laboratory of Biomedical Engineering, PO Box 2200, FIN–02015 HUT, Finland
[2] Helsinki University of Technology, Institute of Mathematics, PO Box 1100, FIN–02015 HUT, Finland

E-mail: Jenni.Heino@hut.fi and Erkki.somersalo@hut.fi

Received 14 September 2001, in final form 11 March 2002
Published 8 April 2002
Online at stacks.iop.org/IP/18/559

Abstract

In this paper we present a model for anisotropic light propagation and reconstructions of optical absorption coefficient in the presence of anisotropies. To model the anisotropies, we derive the diffusion equation in an anisotropic case, and present the diffusion matrix as an eigenvalue decomposition. The inverse problem considered in this paper is to estimate the optical absorption when the directions of anisotropy are known, but the strength may vary. To solve this inverse problem, two approaches are taken. First, we assume that the strength of anisotropy is known, and compare maximum *a posteriori* reconstructions using a fixed value for the strength when the value for the strength is both correct and incorrect. We then extend the solution to allow an uncertainty of the strength of the anisotropy by choosing a prior distribution for the strength and calculating the marginal posterior density. Numerical examples of maximum *a posteriori* estimates are again presented. The results in this paper suggest that the anisotropy of the body is a property that cannot be ignored in the estimation of the absorption coefficient.

1. Introduction

Optical tomography is a promising non-invasive imaging modality in process industry and medical applications [1]. The advantages of optical tomography over existing radiological techniques in medical applications are clear: being non-ionizing, the near-infrared radiation is completely harmless for the patient. Thus, optical tomography enables long-term monitoring of the patients and acquisition of functional information. Also, the relatively light instrumentation allows low-cost portable devices.

Several human tissue types, such as brain and muscles, have optical properties that depend not only on location but also on direction. It is known from functional magnetic

resonance imaging (MRI) that the axonal fibres in the white matter have strong directionally dependent diffusion properties, and there is a good reason to believe that similar properties show up in the optical regime as well (see [2]). Since the imaging of the human head is one of the main application targets of optical tomography, it is vital to understand how anisotropies affect the performance of the optical tomographic methods. In this work we derive the appropriate equations describing the light scattering in anisotropic milieu and perform preliminary numerical studies of the effect of anisotropy. The inversion of the optical parameters is based on a Bayesian statistical approach.

2. Light propagation and anisotropies

The light propagation in the medium is governed by Maxwell's equations. However, the wavelength in the near-infrared region is so small compared with characteristic distances in the medium that exact wave propagation models are of little use. Therefore, the light propagation is modelled by using the *radiative transfer equation*, also known as the *Boltzmann equation*. This will also be our starting point here. In this section we derive the commonly used diffusion approximation to describe the light propagation in the presence of anisotropies. Although essentially similar to the derivations found in the literature for isotropic media (see e.g. [1]), our presentation has some differences, being applicable in both two and three dimensions.

2.1. Radiative transfer and diffusion

We start by fixing the basic notations and concepts. Let $\Omega \subset \mathbb{R}^m$, $m = 2$ or 3, be a bounded domain with a smooth boundary and connected complement. The two-dimensional case is interesting mostly as a simplified computational model. We consider radiation in the body Ω. Let $\hat{\theta} \in S^{m-1}$ be a direction vector. The *radiation flux density* at $x \in \Omega$ at the time $t \in \mathbb{R}$ to the infinitesimal solid angle $\mathrm{d}s$ in the direction $\hat{\theta}$ is written as

$$\mathrm{d}\vec{J}(x, t, \hat{\theta}) = I(x, t, \hat{\theta})\hat{\theta}\,\mathrm{d}s(\hat{\theta}),$$

where the amplitude $I(x, t, \hat{\theta})$ is called the *radiance*. In the framework of the transport theory (cf [3]), this scalar function satisfies the radiative transfer equation,

$$\frac{1}{c}I_t(x, t, \hat{\theta}) + \hat{\theta} \cdot \nabla I(x, t, \hat{\theta}) + (\mu_a(x) + \mu_s(x))I(x, t, \hat{\theta}) - \mu_s(x)\int_{S^{m-1}} f(x, \hat{\theta}, \hat{\omega})I(x, t, \hat{\omega})\,\mathrm{d}s(\hat{\omega}) = q(x, t, \hat{\theta}), \tag{1}$$

where c is the speed of light (assumed to be constant) and the scalar functions μ_a and μ_s are the scattering and absorption coefficients, respectively. The kernel f is the *scattering phase function*, satisfying

$$\int_{S^{m-1}} f(x, \hat{\theta}, \hat{\omega})\,\mathrm{d}s(\hat{\theta}) = \int_{S^{m-1}} f(x, \hat{\theta}, \hat{\omega})\,\mathrm{d}s(\hat{\omega}) = 1 \tag{2}$$

and the reciprocity relation $f(x, \hat{\theta}, \hat{\omega}) = f(x, -\hat{\omega}, -\hat{\theta})$. Finally, q denotes the source term. The material is *isotropic* if the scattering phase depends only on the angle between the incoming and outgoing directions, i.e. $f(x, \hat{\theta}, \hat{\omega}) = h(x, \hat{\theta} \cdot \hat{\omega})$ for some function h. In this paper, our main interest is in *anisotropic media* where the above condition does not hold.

Given the radiation flux density, the flux through an infinitesimal oriented surface patch $\hat{a}\,\mathrm{d}S$, $\hat{a}$ being a unit vector normal to the surface patch, is obtained by integrating the flux

density over all radiation directions,

$$\begin{aligned} \mathrm{d}\Phi(x,t) &= \left(\int_{S^{m-1}} \mathrm{d}\vec{J}(x,t,\hat{\theta})\right)\cdot\hat{a}\,\mathrm{d}S = \left(\int_{S^{m-1}} I(x,t,\hat{\theta})\hat{\theta}\,\mathrm{d}s(\hat{\theta})\right)\cdot\hat{a}\,\mathrm{d}S \\ &= \vec{J}(x,t)\cdot\hat{a}\,\mathrm{d}S, \end{aligned} \tag{3}$$

where the vector field $\vec{J}$ is the *energy current density*. For later use, we also define the *energy fluence*

$$\varphi(x,t) = \int_{S^{m-1}} I(x,t,\hat{\theta})\,\mathrm{d}s(\hat{\theta}). \tag{4}$$

Being an integro-differential equation, the RTE leads easily to numerical problems of prohibitive size if no simplifications are made. The commonly used simplification that is justified at least in strongly scattering media is the *diffusion approximation*. Since this approximation is discussed in the literature mostly in isotropic media, a brief derivation is included below. Our approach differs slightly from the earlier ones. In particular, we make no explicit reference to the spherical harmonics in our derivation.

Let $L^2(S^{m-1})$ denote the space of square integrable functions over the unit sphere S^{m-1} of $\mathbb{R}^m$, and for $\hat{\theta} = (\theta_1, \ldots, \theta_m) \in S^{m-1}$ denote

$$H_1 = \mathrm{sp}\{1, \theta_j,\ 1 \leqslant j \leqslant m\} \subset L^2(S^{m-1}),$$

the subspace spanned by the zeroth and first-order polynomials. Since polynomials of degree less than or equal to unity are harmonic in $\mathbb{R}^m$, H_1 is in fact equal to the space spanned by the spherical harmonics of order unity or less. A simple variational argument shows that the orthogonal projection $P : L^2(S^{m-1}) \to H_1$ is given as

$$Pf(\hat{\theta}) = \frac{1}{|S^{m-1}|}\left(\int_{S^{m-1}} f(\hat{\theta})\,\mathrm{d}s + m\hat{\theta}\ \cdot \int_{S^{m-1}} \hat{\theta} f(\hat{\theta})\,\mathrm{d}s\right), \tag{5}$$

where $|S^{m-1}|$ denotes the surface measure of the sphere. In terms of the flux density (3) and energy fluence (4), the P_1-approximation of the radiance I is

$$I(x,t,\hat{\theta}) \approx PI(x,t,\hat{\theta}) = \frac{1}{|S^{m-1}|}(\varphi(x,t) + m\vec{J}(x,t)\cdot\hat{\theta}). \tag{6}$$

Consider the RTE (1), written for short as $\mathcal{B}I = q$, where $\mathcal{B}$ denotes the integro-differential operator on the left side of the equation (1). The P_1 approximation of the radiative transfer equation (1) is defined as

$$P\mathcal{B}PI = Pq. \tag{7}$$

By substituting the approximation (6) in this equation and applying the projection P on both sides of the equation, we find by a straightforward integration that the equation (7) assumes the form

$$\begin{aligned} P\mathcal{B}(\varphi + m\vec{J}\cdot\hat{\theta}) &= \left(\frac{1}{c}\varphi_t + \mu_a\varphi + \nabla\cdot\vec{J}\right) + m\left(\frac{1}{c}\vec{J}_t + \frac{1}{m}\nabla\varphi + (\mu_a + \mu_s(1-B))\vec{J}\right)\cdot\hat{\theta} \\ &= q_0(x,t) + m\vec{q}_1(x,t)\cdot\hat{\theta}, \end{aligned} \tag{8}$$

where $B = B(x) \in \mathbb{R}^{m\times m}$ is the matrix with elements

$$B_{i,j}(x) = \frac{m}{|S^{m-1}|}\int_{S^{m-1}}\int_{S^{m-1}} \theta_i\omega_j f(x,\hat{\theta},\hat{\omega})\,\mathrm{d}s(\hat{\theta})\,\mathrm{d}s(\hat{\omega}), \tag{9}$$

and the source terms are simply

$$q_0(x,t) = \int_{S^{m-1}} q(x,t,\hat{\theta})\,\mathrm{d}s(\hat{\theta}), \qquad \vec{q}_1(x,t) = \int_{S^{m-1}} \hat{\theta}q(x,t,\hat{\theta})\,\mathrm{d}s(\hat{\theta}).$$

Observe that by the positivity of f, the condition (2) and Schwarz inequality, we have

$$|\vec{v}\cdot B\vec{v}| \leqslant \frac{m}{|S^{m-1}|}\left(\int_{S^{m-1}}(\vec{v}\cdot\hat{\theta})^2\,\mathrm{d}S\right)^{1/2}\left(\int_{S^{m-1}}(\vec{v}\cdot\hat{\omega})^2\,\mathrm{d}S\right)^{1/2} \leqslant \|v\|^2. \quad (10)$$

Equation (8) should apply for all directions $\hat{\theta}$, so we have the system

$$\frac{1}{c}\varphi_t = -\nabla\cdot\vec{J} - \mu_a\varphi + q_0, \quad (11)$$

$$\frac{1}{c}\vec{J}_t = -\frac{1}{m}\nabla\varphi - (\mu_a + (1-B)\mu_s)\vec{J} + \vec{q}_1. \quad (12)$$

This coupled hyperbolic system could be used as such to describe the light propagation. A further simplification is attained if we can argue that above

$$\frac{1}{c}\vec{J}_t \approx 0. \quad (13)$$

With this approximation, equation (12) reduces to an equivalent of *Fick's law*,

$$\vec{J} = -\kappa\nabla\varphi + m\kappa\vec{q}_1, \qquad \kappa = \frac{1}{m}(\mu_a + (1-B)\mu_s)^{-1} \in \mathbb{R}^{m\times m}. \quad (14)$$

A substitution into equation (11) leads to an equation of parabolic type, a *diffusion equation*

$$\frac{1}{c}\varphi_t = \nabla\cdot\kappa\nabla\varphi - \mu_a\varphi + Q, \qquad Q = q_0 - m\nabla\cdot\kappa\vec{q}_1. \quad (15)$$

Notice that due to (10) the diffusion coefficient κ is in general a positive definite symmetric matrix, and it is of the form $\kappa = \rho I$, where $\rho = \rho(x)$ is a scalar function

$$\rho = \frac{1}{m}(\mu_a + \mu_s')^{-1}, \qquad \mu_s' = (1-g)\mu_s, \quad (16)$$

and $g = g(x)$ is

$$g = \frac{1}{|S^{m-1}|}\int_{S^{m-1}}\int_{S^{m-1}} h(x,\hat{\theta}\cdot\hat{\omega})(\hat{\theta}\cdot\hat{\omega})\,\mathrm{d}s(\hat{\theta})\,\mathrm{d}s(\hat{\omega}) = \frac{1}{m}\operatorname{Tr} B, \quad (17)$$

if the material is isotropic.

2.2. Boundary conditions and the source model

In this section it is the aim to describe the boundary conditions of a body with strong scattering as well as to specify the boundary data and source model in optical tomography. There are some differences between our discussion and some of the existing literature, so the details are included below.

In the following, the exterior unit normal vector at $x \in \partial\Omega$ is denoted by $\hat{n} = \hat{n}(x)$. We start by specifying the inward and outward flux densities (Φ_- and Φ_+, respectively) at the boundary in terms of the P_1 approximation. The total flux inwards at $x \in \partial\Omega$ within the P_1 approximation is given as

$$\begin{aligned}\Phi_-(x,t) &= \int_{\{\hat{n}(x)\cdot\hat{\theta}<0\}} \mathrm{d}\vec{J}\,(x,t,\hat{\theta}) \\ &\approx \frac{1}{|S^{m-1}|}\int_{\{\hat{n}(x)\cdot\hat{\theta}<0\}}(\varphi(x,t) + m\vec{J}(x,t)\cdot\hat{\theta})\hat{\theta}\cdot\hat{n}(x)\,\mathrm{d}s(\hat{\theta}).\end{aligned}$$

By using the spherical coordinates of $\mathbb{R}^m$, we obtain

$$\int_{\{\hat{n}\cdot\hat{\theta}<0\}}\hat{\theta}\cdot\hat{n}\,\mathrm{d}s = -|S^{m-2}|\int_0^1 t(1-t^2)^{(m-3)/2}\,\mathrm{d}t = -\frac{|S^{m-2}|}{m-1}.$$

To integrate the second term, we divide $\vec{J}$ into parts perpendicular and parallel to the surface $\partial\Omega$,

$$\vec{J} = (\vec{J}\cdot\hat{n})\hat{n} + \vec{J}_\perp, \qquad \hat{n}\cdot\vec{J}_\perp = 0.$$

Then,

$$\int_{\{\hat{n}\cdot\hat{\theta}<0\}} (\vec{J}\cdot\hat{\theta})(\hat{\theta}\cdot\hat{n})\,\mathrm{d}s = (\vec{J}\cdot\hat{n})\int_{\{\hat{n}\cdot\hat{\theta}<0\}} (\hat{n}\cdot\hat{\theta})^2\,\mathrm{d}s + \int_{\{\hat{n}\cdot\hat{\theta}<0\}} (\hat{\theta}\cdot\vec{J}_\perp)(\hat{\theta}\cdot\hat{n})\,\mathrm{d}s.$$

The latter integral vanishes due to the antisymmetry of the integrand in the plane perpendicular to $\hat{n}$. To evaluate the former integral, we write

$$\int_{\{\hat{n}\cdot\hat{\theta}<0\}} (\hat{\theta}\cdot\hat{n})^2\,\mathrm{d}s = \frac{1}{2}\int_{S^{m-1}} (\hat{n}\cdot\hat{\theta})^2\,\mathrm{d}s = \frac{|S^{m-1}|}{2m}$$

by symmetry. Taking into account the formula $|S^{m-1}| = 2\pi^{m/2}/\Gamma(m/2)$, we have

$$\Phi_- = \frac{1}{|S^{m-1}|}\left(-\frac{|S^{m-2}|}{m-1}\varphi + m(\vec{J}\cdot\hat{n})\frac{|S^{m-1}|}{2m}\right) = -\gamma\varphi + \frac{1}{2}\hat{n}\cdot\vec{J},$$

where

$$\gamma = \gamma_m = \frac{\Gamma(m/2)}{\sqrt{\pi}(m-1)\Gamma((m-1)/2)}.$$

In dimensions $m = 2$ and 3, the dimension-dependent constant γ obtains values $\gamma_2 = 1/\pi$, $\gamma_3 = 1/4$.

Similarly, the outward flux is obtained by switching the direction of the normal, yielding

$$\Phi_+ = \gamma\varphi + \tfrac{1}{2}\hat{n}\cdot\vec{J}. \tag{18}$$

Assume that the body is illuminated from outside by specified light sources. At $x \in \partial\Omega$, the total flux inwards must be equal to the input flux $\Phi_{\mathrm{in}}(x)$ from the outside source plus the reflected photon flux due to the refractive index mismatch across the boundary $\partial\Omega$. Let us denote by $R = R(x)$, $0 \leqslant R \leqslant 1$, the reflection coefficient at $x \in \partial\Omega$. By assuming that the boundary condition describing the reflection is local, we may write

$$\Phi_-(x,t) = R(x)\Phi_+(x,t) + \Phi_{\mathrm{in}}(x,t),$$

or

$$\Phi_{\mathrm{in}} = -(1+R)\gamma\varphi - \tfrac{1}{2}(1-R)\hat{n}\cdot\kappa\nabla\varphi. \tag{19}$$

On the other hand, the total flux density out of the body is reduced by the amount of reflected flux due to the refractive index mismatch, i.e.

$$\Phi_{\mathrm{out}}(x,t) = (1-R(x))\Phi_+(x,t). \tag{20}$$

The boundary data of the optical tomography could be specified as all possible pairs $(\Phi_{\mathrm{in}}, \Phi_{\mathrm{out}})$ along the boundary. In practice, however, the situation is slightly more involved. The boundary sources are typically pointwise optical fibre sources attached on the surface of the body, and it is evident that right under the source the diffusion approximation is quite inaccurate. For a better agreement with actual measurements, we adopt an approximation that was used for example in the articles [4, 5] and [1]. The light source is modelled as a collimated pencil beam perpendicular to the surface. This source is represented by an effective point source under the optical fibre inside the body, and for the input flux Φ_{in} we assume that $\Phi_{\mathrm{in}} = 0$ throughout the boundary $\partial\Omega$. Effectively, this leads to a Robin type boundary condition

$$\varphi + h\hat{n}\cdot\kappa\nabla\varphi = 0, \qquad h = \frac{1-R}{2\gamma(1+R)}, \tag{21}$$

and the source term

$$Q(x,t) = \sum_{\ell=1}^{L} Q_\ell(t)\delta(x - x_\ell).$$

Here, L is the number of boundary sources and x_ℓ is a point at the distance $d \sim 1/\mu_s'$ below the ℓth boundary source, while Q_ℓ determines the source pattern. There is a vast literature on the reflection coefficients, in particular in connection to the transport theory (see e.g. [1, 6] and references therein). In this paper, we use $R = 0$ in the numerical simulations. Typically, one boundary source is activated at a time. Typical source patterns are short delta pulses or continuous wave patterns with harmonic modulation. In this work, we consider the latter. Hence, assuming that only the kth boundary source is activated, and the time dependence is harmonic with angular frequency $\omega > 0$, we have

$$Q(x,t) = Q^{(k)}(x,t) = Q_0 \mathrm{e}^{-\mathrm{i}\omega t}\delta(x - x_k).$$

By writing the corresponding solution of the diffusion equation as $\varphi(x,t) = \varphi^{(k)}(x)\mathrm{e}^{-\mathrm{i}\omega t}$, we have the elliptic equation

$$\nabla \cdot \kappa \nabla \varphi^{(k)} - \mu_a' \varphi^{(k)} = Q_0 \delta(x - x_k), \tag{22}$$

where $\mu_a' = \mu_a - \mathrm{i}k, k = \omega/c$. We recall that in the time-harmonic case, the approximation (13) is not necessary. Without this approximation, one needs to replace μ_a by μ_a' in the diffusion matrix κ (formula (14)). This correction may be significant especially at high modulation frequencies.

The numerical approximation of the forward solution is based on finite-element computation. Therefore, we write the variational form of the equation (22) with the boundary condition (21) included. By multiplying the equation (22) with a test function ψ and by intergrating by parts over Ω, we arrive at the variational equation

$$\int_\Omega \nabla\psi \cdot \kappa \nabla \varphi^{(k)}\,\mathrm{d}x + \int_\Omega \mu_a' \psi \varphi^{(k)}\,\mathrm{d}x + \int_{\partial\Omega} \frac{1}{h}\psi\varphi\,\mathrm{d}S = -Q_0\psi(x_k), \tag{23}$$

where the Robin boundary condition (21) was taken into account.

The boundary data consist of the measured outward flux at points on $\partial\Omega$ where optical fibres are fixed. If $y_j \in \partial\Omega$ is a boundary point corresponding to the optical fibre location, the measured outward flux $\Phi_{\mathrm{out}}^{(k)}$ corresponding to the kth boundary source activated, by taking into account formulae (20), (18) and (14) as well as the boundary condition (21), is simply

$$\Phi_{\mathrm{out}}(y_j) = 2\gamma\varphi^{(k)}(y_j). \tag{24}$$

In numerical simulations, we assume that the data consist of the noisy observation of the logarithm of the amplitude and the complex phase.

3. Anisotropy model and numerical approximation

In this section we confine the discussion in the two-dimensional case corresponding to the numerical examples in this work.

Assume that the domain Ω is divided into finite elements Δ_j, and we approximate the solution $\phi^{(k)}$ by means of nodal-based basis functions,

$$\varphi(x) \approx \sum_{j=1}^{N_{\mathrm{n}}} \alpha_j \psi_j(x). \tag{25}$$

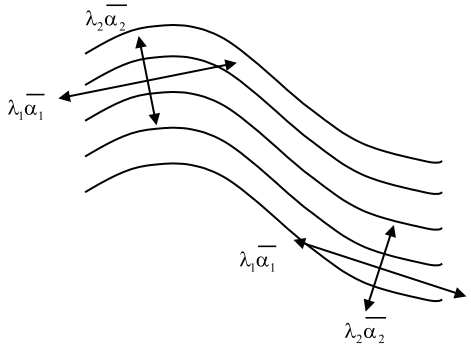

Figure 1. A schematic illustration of the representation of anisotropy using eigenvalue decomposition. The direction of anisotropic structures is presented by two orthogonal directions confined in the matrix $U(x) = [\vec{\alpha}_1(x), \vec{\alpha}_2(x)]$ and the strength by the corresponding eigenvalues $\lambda_1(x), \lambda_2(x)$.

Here, N_{n} is the number of nodes in the finite-element mesh. By choosing the test function ψ in (23) to be one of the basis functions, we arrive at the matrix equation

$$A\alpha^{(k)} = \beta^{(k)}, \tag{26}$$

where A is the $N_{\mathrm{n}} \times N_{\mathrm{n}}$ symmetric matrix with entries

$$A_{j,\ell} = \int_\Omega \nabla\psi_j \cdot \kappa \nabla\psi_\ell \,\mathrm{d}x + \int_\Omega \mu_a' \psi_j \psi_\ell \,\mathrm{d}x + \int_{\partial\Omega} \frac{1}{h} \psi_j \psi_\ell \,\mathrm{d}S, \tag{27}$$

and $\beta^{(k)}$ is an N_{n}-vector,

$$\beta_j^{(k)} = -Q_0 \psi_j(x_k). \tag{28}$$

Consider the anisotropy matrix $B = B(x) \in \mathbb{R}^{2\times 2}$ defined in (9). We write the eigenvalue decomposition as

$$B(x) = U(x)\mathrm{diag}(b_1(x), b_2(x))U(x)^{\mathrm{T}},$$

where $U(x) \in \mathbb{R}^{2\times 2}$ is an orthogonal matrix and we assume that the eigenvalues $b_j(x)$ are positive. This decomposition leads to a corresponding decomposition of the diffusion matrix κ,

$$\kappa(x) = U(x)\mathrm{diag}(\lambda_1(x), \lambda_2(x))U(x)^{\mathrm{T}},$$

where

$$\lambda_j(x) = \frac{1}{2(\mu_a(x) + (1 - b_j(x))\mu_s(x))}, \qquad j = 1, 2 \tag{29}$$

(see figure 1).

Consider the system matrix A defined in (27). By writing

$$U(x)^{\mathrm{T}} \nabla\psi_j(x) = \xi_j(x)\hat{e}_1 + \eta_j(x)\hat{e}_2,$$

where the vectors $\hat{e}_j$ are the Cartesian basis vectors, we obtain

$$\int_\Omega \nabla\psi_j \cdot \kappa \nabla\psi_\ell \,\mathrm{d}x = \int_\Omega \lambda_1 \xi_j \xi_\ell \,\mathrm{d}x + \int_\Omega \lambda_2 \eta_j \eta_\ell \,\mathrm{d}x.$$

This expression becomes particularly simple if we assume that the *strength* of the anisotropy is constant, i.e.

$$\lambda_j(x) = \lambda_j = \text{constant}, \qquad j = 1, 2.$$

Note that this assumption does not mean that the diffusion coefficient is constant, since the principal directions coded in the matrix $U(x)$ may vary. In this case,

$$\int_\Omega \nabla\psi_j \cdot \kappa \nabla\psi_k \, \mathrm{d}x = \lambda_1 \int_\Omega \xi_j \xi_k \, \mathrm{d}x + \lambda_2 \int_\Omega \eta_j \eta_k \, \mathrm{d}x. \tag{30}$$

This is the model to be considered in this work. Let us make one further simplifying approximation: we assume in the following that the anisotropy factors λ_j, $j = 1, 2$, are independent of the absorption coefficient. This assumption, although not correct, can be justified when the material is scattering dominated, i.e. $\mu_a \ll \mu_s$, so in formula (29) the absorption coefficient can be ignored.

4. Inverse problem

In this section we consider the following anisotropic inverse problem of optical tomography. Assume that we know the principal directions of the anisotropy of the diffusion matrix κ, but the strength (λ_1, λ_2) of the anisotropy is poorly known. The goal is to estimate the absorption coefficient $\mu_a = \mu_a(x)$ based on optical boundary measurements.

Before going into details, let us justify the formulation of the above inverse problem. First, if no information on the anisotropic structure is available, one can show that the inverse problem of determining simultaneously the diffusion matrix and the absorption coefficient from the boundary data has no unique solution even when the boundary data are noiseless and complete. The non-uniqueness issue is not discussed in this article. On the other hand, it may be possible to make some inference of the principal directions of structural anisotropies in human tissue, for example based on anatomical information or other imaging modalities such as functional MRI (diffusion tensor imaging; see [7]). Of course, this type of information is never accurate, so our study must be considered as a preliminary one. We point out that the correlation between optical and diffusion anisotropies is not an experimentally verified fact. However, they both depend on the structural anisotropy of the matter. Indeed, Monte Carlo simulations indicate that structural anisotropy gives rise to optical anisotropy (see [2]).

Our approach to the inverse problem is based on Bayesian statistical analysis that is briefly reviewed here. For more detailed discussion, we refer e.g. to [8, 9] and references therein. To avoid computational difficulties, rather restrictive approximations of the statistics of the random variables are made in this paper.

Let y denote a vector that consists of the single real-valued observations at the body's boundary. As explained at the end of section 2, these observations may be the logarithm of the amplitude and/or the phase angle of the outward flux at given boundary points with different excitations. Assuming additive measurement noise, the observation model is written as

$$y = G(\mu_a, \lambda) + n,$$

where $G(\mu_a, \lambda)$ is the model for the noiseless observation. Here, μ_a is a vector consisting of the discrete values of the absorption coefficient in the pixels and $\lambda = (\lambda_1, \lambda_2)$ defines the anisotropy.

Assume that the probability density $\pi_{\text{noise}}(n)$ of the noise is known. Further, let $\pi_{\text{pr}}(\mu_a, \lambda)$ denote the prior density of the variables μ_a and λ. Assuming that the noise n is independent of μ_a and λ, the Bayes formula for the posterior probability density gives

$$\pi(\mu_a, \lambda | y) \sim \pi_{\text{pr}}(\mu_a, \lambda)\pi_{\text{noise}}(y - G(\mu_a, \lambda)).$$

In this work, we approximate the distribution of the noise by a zero-mean Gaussian, i.e. we assume that $n \sim \mathcal{N}(0, \Gamma_{\text{noise}})$, where Γ_{noise} is the noise covariance. The prior distributions

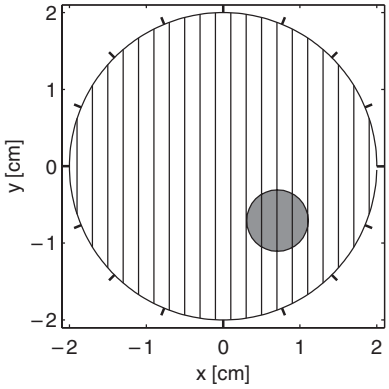

Figure 2. The two-dimensional model used for data generation consists of a homogeneous sphere (radius 2 cm) with a single spherical perturbation (radius 4 mm) in the absorption coefficient. For μ_s, we use a constant value of 200 cm^{-1}, and for μ_a 0.25 cm^{-1} in the background and 1 cm^{-1} in the perturbation. In the anisotropic case, the direction of the anisotropy (i.e. $\vec{\alpha}_1$) is chosen parallel to the y-axis. Sixteen source and measurement locations are denoted on the boundary. The source is placed at each location at turn, and the rest of the locations are used for measurement, resulting in 240 data values.

are also chosen to be Gaussian, and we assume for simplicity that μ_a and λ are mutually independent. By writing $\mu_a \sim \mathcal{N}(\mu_{a0}, \Gamma_\mu)$ and $\lambda \sim \mathcal{N}(\lambda_0, \Gamma_\lambda)$, we obtain

$$\pi(\mu_a, \lambda|y) \sim \exp(-\tfrac{1}{2}((y - G(\mu_a, \lambda))^{\mathrm{T}}\Gamma_{\mathrm{noise}}^{-1}(y - G(\mu_a, \lambda)) + (\mu_a - \mu_{a0})^{\mathrm{T}}\Gamma_\mu^{-1}(\mu_a - \mu_{a0}) + (\lambda - \lambda_0)^{\mathrm{T}}\Gamma_\lambda^{-1}(\lambda - \lambda_0))). \tag{31}$$

This formula is the starting point for the subsequent discussion.

In our first experiments, we investigate how strongly the anisotropy affects the estimation of the absorption coefficient. More precisely, assume that the anisotropy constants λ_j, $j = 1, 2$, are believed to be known. In terms of Bayesian statistics, this belief is tantamount to saying that in the formula (31) the prior covariance $\Gamma_\lambda \to 0$ in the sense of quadratic form, i.e. $\lambda = \lambda_0$ with unit probability. Under this assumption, we calculate the maximum *a posteriori* estimator $\mu_{a,MAP}$ by seeking to minimize the functional

$$\mathcal{F}(\mu_a) = (y - G(\mu_a, \lambda_0))^{\mathrm{T}}\Gamma_{\mathrm{noise}}^{-1}(y - G(\mu_a, \lambda_0)) + (\mu_a - \mu_{a0})^{\mathrm{T}}\Gamma_\mu^{-1}(\mu_a - \mu_{a0}).$$

The minimization is performed in practice by the iterative Gauss–Newton algorithm.

Figure 2 shows a schematic picture of the body that was used in data generation. The direction of the possible anisotropy is indicated by the vertical lines. The values of μ_s and μ_a used in the data generation are indicated in the figure caption and these values are unaltered in our experiments, while the eigenvalue b_2 of the matrix B (formula (9)) is altered, and as a consequence of the formula (29) the value of λ_2 varies. We denote by λ_{true} the true value of the anisotropy vector used in data generation.

Consider first the case where the prior corresponds to an isotropic body, i.e. $\lambda_{0,1} = \lambda_{0,2}$. We compare the maximum *a posteriori* estimates $\mu_{a,\mathrm{MAP}}$ in the case when $\lambda_{\mathrm{true}} = \lambda_0$, i.e. the body is in fact isotropic, and when $\lambda_{\mathrm{true}} \neq \lambda_0$ and the body is anisotropic. In the latter case, the prior is of course flawed.

In figure 3, the maximum *a posteriori* estimates of the absorption coefficient μ_a are depicted in these two cases. The reconstructions are based on the logarithm of the amplitude datatype. In figure 3(*a*), we had $\lambda_0 = \lambda_{\mathrm{true}}$ with $b_1 = b_2 = 0.9$, while in figure 3(*b*) we had λ_0 as above but $b_1 = 0.9$ and $b_2 = 0.7$. The noise covariance was assumed to be $\Gamma_{\mathrm{noise}} = \sigma^2 I$ with the standard deviation σ corresponding to 5% relative noise level of the amplitude. Artificial

noise corresponding to this noise level was added to the computed signal. To avoid 'inverse crimes' the data were generated in a different mesh than the one used in the reconstruction. The forward and inverse meshes consisted of 9155 and 2993 elements, respectively, and had been generated with a bubble mesh generator [10]. The prior covariance of μ_a was chosen of the form $\Gamma_\mu = \alpha I$ with the value of α chosen separately in each case by visual inspection of the reconstruction. For the Gauss–Newton algorithm, a couple of iterations were performed. Since increasing the number of iterations does not alter the results significantly, this was considered sufficient for the purpose of this paper.

Comparing the results in figure 3, we see that when the anisotropy is ignored, the reconstruction is badly distorted. One can see that the effect of the anisotropy is compensated by increased or decreased absorption near the measurement points, depending on their location relative to the direction of the anisotropy.

Next, we consider again two sets of data with different values of λ_{true} (corresponding to the values of $(b_1, b_2) = (0.9, 0.8)$ and $(b_1, b_2) = (0.9, 0.55)$) and with Gaussian noise added, and an anisotropic model with $\lambda = \lambda_0$ (corresponding to $(b_1, b_2) = (0.9, 0.8)$). Figure 4 displays four reconstructions with this model. The upper row presents reconstructions where the data and the prior are in accordance, i.e. $\lambda_0 = \lambda_{\text{true}}$. On the lower row, the prior is flawed, i.e. we have $\lambda_0 \neq \lambda_{\text{true}}$. On the left, the maximum *a posteriori* estimates of the absorption coefficient are based on the logarithm of the amplitude data, and on the right, on the phase data. For the phase data, the value of the standard deviation σ of the noise was approximated to be 1% of the maximum value of the data. On the lower row, an incorrect assumption on the strength of the anisotropy leads to serious distortions in the reconstructions. In this case, the true anisotropy is stronger than that assumed for reconstruction, producing similar effects as in figure 3(*b*).

As the previous examples demonstrated, the background anisotropy cannot be neglected in the estimation of the absorption coefficient. Furthermore, if we fix the anisotropy structure in the model, it is quite critical that the fixed model is the correct one. It is clear, however, that in general we cannot assume accurate values of the of the anisotropy factors to be available. Therefore, we allow an uncertainty of the anisotropy by calculating the marginal posterior density of μ_a, i.e. the probability density

$$\pi(\mu_a|y) = \int \pi(\mu_a, \lambda|y)\,\mathrm{d}\lambda. \tag{32}$$

Assuming that the posterior density is of the form (31), a proper solution would require for example the use of Markov chain Monte Carlo methods to perform the integration (see [9, 11] and references therein). In this work, however, we confine ourselves to a simplifying approximation by linearizing the mapping G around some reference values μ_a^* and λ^*. We write

$$\begin{aligned} G(\mu_a, \lambda) &\approx G(\mu_a^*, \lambda^*) + D_{\mu_a} G(\mu_a^*, \lambda^*)(\mu_a - \mu_a^*) + D_\lambda G(\mu_a^*, \lambda^*)(\lambda - \lambda^*) \\ &= y^* + A_1(\mu_a - \mu_a^*) + A_2(\lambda - \lambda^*) \end{aligned}$$

with obvious notations. With this approximation, both the posterior distribution (31) and the marginal distribution (32) assume a Gaussian form. In the appendix, the derivations of the following formulae are sketched. We have

$$\pi(\mu_a, \lambda|y) \sim \exp\left\{-\tfrac{1}{2}\left(\begin{pmatrix}\mu_a \\ \lambda\end{pmatrix} - \begin{pmatrix}\overline{\mu}_a \\ \overline{\lambda}\end{pmatrix}\right)^{\mathrm{T}} \Gamma_{\text{post}}^{-1}\left(\begin{pmatrix}\mu_a \\ \lambda \\ \lambda\end{pmatrix} - \begin{pmatrix}\overline{\mu}_a \\ \overline{\lambda}\end{pmatrix}\right)\right\}, \tag{33}$$

where the posterior covariance matrix is given as

$$\begin{aligned} \Gamma_{\text{post}} &= \begin{pmatrix}\Gamma_\mu & 0 \\ 0 & \Gamma_\lambda\end{pmatrix} - \begin{pmatrix}\Gamma_\mu A_1^{\mathrm{T}} \\ \Gamma_\lambda A_2^{\mathrm{T}}\end{pmatrix} L \begin{pmatrix} A_1\Gamma_\mu & A_2\Gamma_\lambda \end{pmatrix} \\ &= \begin{pmatrix} \Gamma_\mu - \Gamma_\mu A_1^{\mathrm{T}} L A_1 \Gamma_\mu & \Gamma_\mu A_1^{\mathrm{T}} L A_2 \Gamma_\lambda \\ \Gamma_\lambda A_2^{\mathrm{T}} L A_1 \Gamma_\mu & \Gamma_\lambda - \Gamma_\lambda A_2^{\mathrm{T}} L A_2 \Gamma_\lambda \end{pmatrix}, \end{aligned} \tag{34}$$

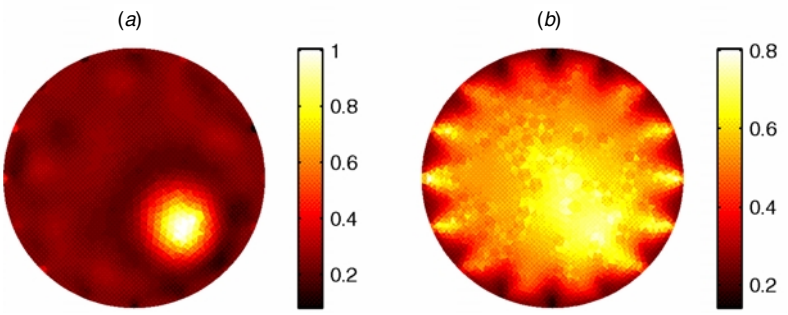

Figure 3. Maximum *a posteriori* estimates of the absorption coefficient using an isotropic model. The data were created (*a*) with an isotropic model using $b = 0.9$ and (*b*) with an anisotropic model using $b_1 = 0.9$ and $b_2 = 0.7$.

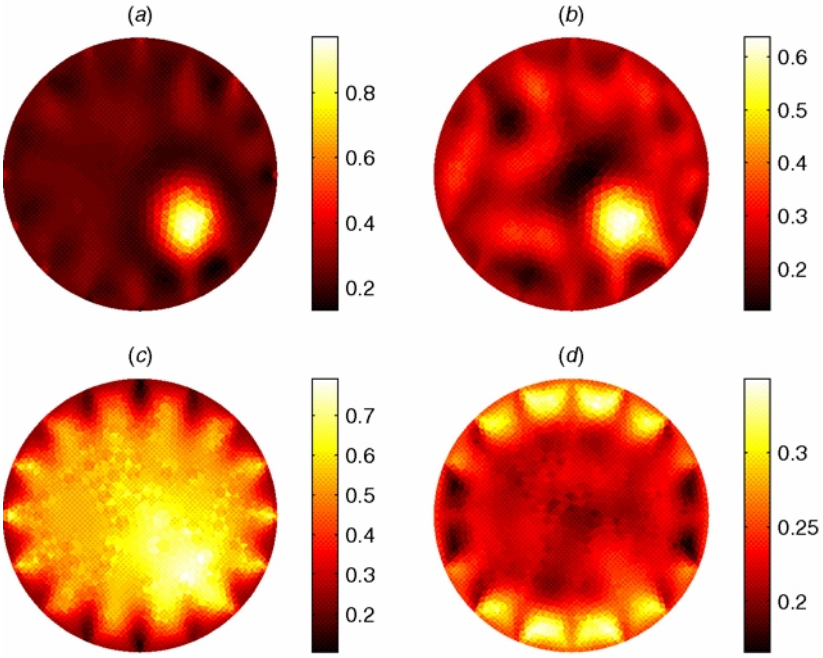

Figure 4. Maximum *a posteriori* estimates of the absorption coefficient based on (*a*), (*c*) logarithm of amplitude and (*b*), (*d*) phase data using an anisotropic model. In the reconstruction, the values of anisotropy are $b_1 = 0.9$ and $b_2 = 0.8$. In (*a*) and (*b*), the data were created using these values; in (*c*) and (*d*), we used $b_1 = 0.9$ and $b_2 = 0.55$.

and

$$L = (A_1\Gamma_\mu A_1^{\mathrm{T}} + A_2\Gamma_\lambda A_2^{\mathrm{T}} + \Gamma_{\mathrm{noise}})^{-1}.$$

The mean values are obtained by the formula

$$\begin{pmatrix} \overline{\mu}_a \\ \overline{\lambda} \end{pmatrix} = \begin{pmatrix} \mu_{a0} \\ \lambda_0 \end{pmatrix} + \begin{pmatrix} \Gamma_\mu A_1^{\mathrm{T}} \\ \Gamma_\lambda A_2^{\mathrm{T}} \end{pmatrix} L(y - y^* - A_1(\mu_{a0} - \mu_a^*) - A_2(\lambda_0 - \lambda^*)).$$

Similarly, the marginal density of μ_a within the linearizing approximation is

$$\pi(\mu_a|y) \sim \exp(-\tfrac{1}{2}(\mu_a - \overline{\mu}_a)^{\mathrm{T}}\Gamma_{\mathrm{post},\mu}^{-1}(\mu_a - \overline{\mu}_a)), \tag{35}$$

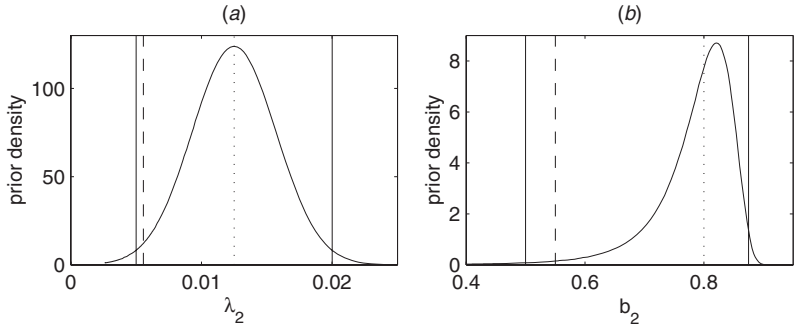

Figure 5. The prior densities of (*a*) λ_2 and (*b*) b_2. The mean values are indicated with dotted vertical lines and the minimum and maximum values with solid lines. The first set of data was computed using the mean value, and the values used for the second data set are indicated with dashed lines.

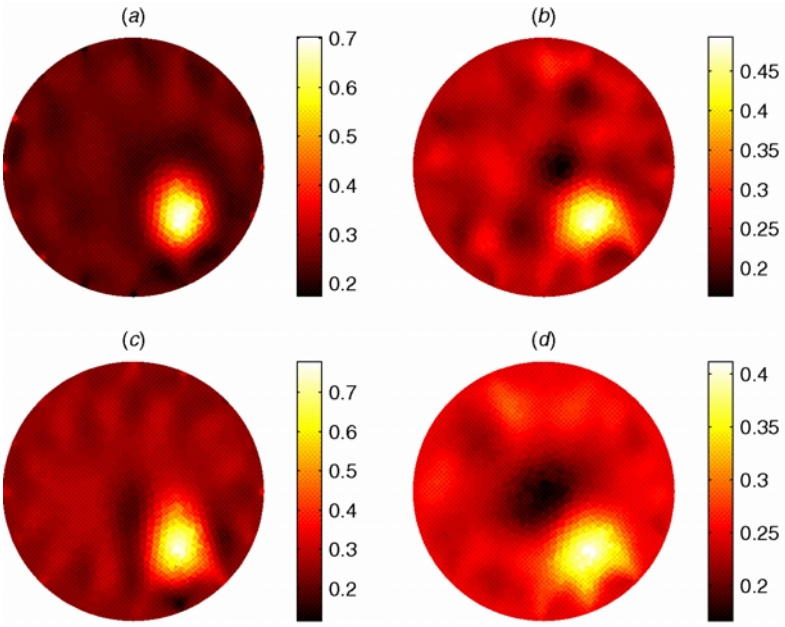

Figure 6. Maximum *a posteriori* estimates of the absorption coefficient from the marginal density after integrating the anisotropy out. Estimates are based on (*a*), (*c*) logarithm of amplitude and (*b*), (*d*) phase data. The data were created in (*a*) and (*b*) using the mean values $(b_1, b_2) = (0.9, 0.8)$ of the prior distribution, and in (*c*) and (*d*) using $(b_1, b_2) = (0.9, 0.55)$.

with $\overline{\mu}_a$ as above, and

$$\Gamma_{\text{post},\mu} = \Gamma_\mu - \Gamma_\mu A_1^{\mathrm{T}}(A_1\Gamma_\mu A_1^{\mathrm{T}} + A_2\Gamma_\lambda A_2^{\mathrm{T}} + \Gamma_{\text{noise}})^{-1}A_1\Gamma_\mu. \tag{36}$$

It is worth noting that, above, the mean values $\overline{\mu}_a$ obtained from the posterior distribution $\pi(\mu_a, \lambda|y)$ and from the marginal distribution $\pi(\mu_a|y)$ coincide due to the Gaussian approximations and linearizations. In general, this is not the case.

In our numerical experiments we consider the case where λ has a Gaussian prior, $\lambda \sim \mathcal{N}(\lambda_0, \Gamma_\lambda)$, where $\Gamma_\lambda = \text{diag}(\sigma_1^2, \sigma_2^2)$. For simplicity, it is assumed here that one of the anisotropy parameters, say λ_1, is rather well known. This is effectuated by choosing σ_1^2 very

small, i.e. $\lambda_1 \approx \lambda_{0,1}$ with a probability close to unity. We emphasize that there are no physical grounds for the assumption that λ_1 is well known and this is done purely for computational convenience. Also, the general Bayesian approach applies without this assumption. To fix a value for σ_2, we choose a plausible interval $[b_{2,\min}, b_{2,\max}]$, calculate the corresponding limit values $\lambda_{2,\min}$ and $\lambda_{2,\max}$ by formula (29) and adjust σ_2 so that the probabilities $\lambda_2 < \lambda_{2,\min}$ and $\lambda_2 > \lambda_{2,\max}$ are both equal to 0.01. The prior density for b_2 can be calculated from the dependence between λ and b. Figure 5 shows the prior densities of λ_2 and b_2. The numerical values in this simulation were chosen so that λ_0 corresponds to $(b_1, b_2) = (0.9, 0.8)$ and $(b_{2,\min}, b_{2,\max}) = (0.5, 0.875)$. Note that the choices for $(b_{2,\min}, b_{2,\max})$ are in accordance with the mean value chosen. The minimum, maximum and mean values are indicated in the figure.

In solving the inverse problem, the point of the linearization was chosen to coincide with the mean value of the prior distribution, i.e. we set $(\mu_a^*, \lambda^*) = (\mu_{a0}, \lambda_0)$. To test the method, we generate two sets of data: in the first one, the true value of λ corresponds to the anisotropy eigenvalues $(b_1, b_2) = (0.9, 0.8)$. In the second case, we set λ_{true} to correspond to the values $(b_1, b_2) = (0.9, 0.55)$. Observe that in the first case b_2 is drawn close to the maximum of the prior distribution of b_2, while in the latter case it is drawn from the very tail, as indicated in figure 5.

Figure 6 displays the maximum *a posteriori* estimates, i.e. the mean values, of the absorption coefficient from the marginal density. These estimates are comparable to the estimates in figure 4 where the value of anisotropy is fixed. On the left, the estimates are based on the logarithm of the amplitude data, and on the right, on the phase data. On the upper row, the first data set corresponding to the mean values of the prior distribution is used. The dynamical range of the reconstructions is slightly reduced compared with the case of fixed value of anisotropy, but this could be helped by performing more iterations as in figure 4. The lower row displays estimates using the second data set corresponding to the case $\lambda_0 \neq \lambda_{\text{true}}$. In this case, the estimates from the marginal density are clearly better than those obtained using a fixed value of anisotropy.

The marginal posterior density of the absorption coefficient in a single pixel is easily obtained from the marginal density (35). Hence, we can investigate the effect of changing the standard deviation σ_2 in the prior distribution of λ_2 on the marginal density of the solution in a single pixel. It turns out that changing the value of σ_2 within reasonable limits (i.e. σ_2 is not clearly too small corresponding to the case of fixed value of λ_2) changes the mean value of the solution slightly, but does not seem to alter the shape of the marginal density significantly. In this sense the method is rather robust to the value of σ_2, which is, after all, a parameter chosen quite randomly.

Remark. The computations presented in this paper have also been conducted using a different smoothing prior for the absorption coefficient. In this case, the prior covariance Γ_μ corresponds to a second-order smoothness prior, i.e. $\Gamma_\mu^{-1} = \alpha L^{\mathrm{T}} L$, where $\alpha > 0$ and L is a discrete approximation of the Laplacian. (For details of how this approximation is computed in an unstructured finite-element mesh, see [9].) The results show a very similar behaviour as presented in this paper. However, for the example case of this paper, the smoothing prior is not the best choice, but it could be successfully applied on cases of smoother variations in the absorption coefficient.

5. Conclusions

Based on the results presented in this paper, the anisotropy of the body is a property that cannot be ignored in the estimation of the absorption coefficient. If the anisotropy model is fixed,

it is crucial for successful estimation of the absorption that this model is correct. In general, however, we cannot assume to have good knowledge of the anisotropy. In some cases prior knowledge of the directions of the anisotropy could be retrieved, for example from diffusion tensor images from diffusion-weighted MRI. However, the uncertainty of the strength of the anisotropy compromises the reconstruction considerably. In this paper, to solve this problem we investigated a case where one of the anisotropy factors was unknown and integrated out, improving the results dramatically. Based on this work, direct comparison of the numerical complexity between the cases where anisotropy is known or integrated out is difficult, since in the latter case we used linearization and the densities were Gaussian, while in the former model non-linear iterative optimization was used. The fully non-linear modelling of anisotropies requires Monte Carlo integration and the computational task becomes considerably heavier. The non-linear modelling is postponed to future work. Another subject of future work is to reconstruct the anisotropy factors simultaneously with the absorption coefficient. Further studies concerning the uncertainties in the anisotropy direction need to be performed.

Acknowledgments

This work was supported by the Academy of Finland, the Foundation of Technology and the Finnish Cultural Foundation. The author JH would like to thank Dr J Nenonen, Helsinki University of Technology, for supporting her work. The authors wish to thank the referees for careful reading of the manuscript and for their valuable comments.

Appendix

In this appendix, we sketch the derivation of the formulae (33) and (35) of the posterior and marginal densities.

Let x_1 and x_2 be two Gaussian random variables with means and covariances $\mathrm{E}x_j = x_{j,0}$ and $\mathrm{E}(x_i - x_{i,0})(x_j - x_{j,0})^{\mathrm{T}} = \Gamma_{ij}$. We assume that the autocovariances Γ_{11} and Γ_{22} are invertible. The joint probability distribution is then of the form

$$\pi(x_1, x_2) \sim \exp\left\{-\tfrac{1}{2}\begin{pmatrix} x_1 - x_{1,0} \\ x_2 - x_{2,0} \end{pmatrix}^{\mathrm{T}} \begin{pmatrix} \Gamma_{11} & \Gamma_{12} \\ \Gamma_{21} & \Gamma_{22} \end{pmatrix}^{-1} \begin{pmatrix} x_1 - x_{1,0} \\ x_2 - x_{2,0} \end{pmatrix}\right\}. \tag{37}$$

By a straightforward Gauss elimination, we find that the inverse of the joint covariance matrix can be written as

$$\Gamma^{-1} = \begin{pmatrix} \tilde{\Gamma}_{22}^{-1} & -\tilde{\Gamma}_{22}^{-1}\Gamma_{12}\Gamma_{22}^{-1} \\ -\tilde{\Gamma}_{11}^{-1}\Gamma_{21}\Gamma_{11}^{-1} & \tilde{\Gamma}_{11}^{-1} \end{pmatrix}, \tag{38}$$

where the Schur complements $\tilde{\Gamma}_{jj}$ are given as $\tilde{\Gamma}_{11} = \Gamma_{22} - \Gamma_{21}\Gamma_{11}^{-1}\Gamma_{12}$ and $\tilde{\Gamma}_{22}$ similarly by interchanging the indices. By substituting this formula into (37) and completing to squares with respect to x_1, we find that

$$\pi(x_1|x_2) \sim \exp\{-\tfrac{1}{2}(x_1 - \overline{x}_1)^{\mathrm{T}}\tilde{\Gamma}_{22}^{-1}(x_1 - \overline{x}_1)\}, \tag{39}$$

with

$$\overline{x}_1 = x_{1,0} + \Gamma_{12}\Gamma_{22}^{-1}(x_2 - x_{2,0}).$$

Formula (33) now follows by choosing $x_1 = (\mu_a, \lambda)$ and $x_2 = y$. The correlation matrix Γ is calculated by using the linearized model

$$y = y^* + A_1(\mu_a - \mu_a^*) + A_2(\lambda - \lambda^*) + n,$$

and taking into account the assumption that μ_a, λ and n are mutually independent.

To derive the formula (35) for the marginal density, consider again formula (37) with $x_1 = \mu_a$, $x_2 = \lambda$. In this interpretation, the joint probability density is the posterior density, i.e. $\pi(x_1, x_2) = \pi(\mu_a, \lambda|y)$ and $\Gamma = \Gamma_{\text{post}}$ given by formula (34). Without loss of generality, we may assume here that $x_{1,0} = 0$, $x_{2,0} = 0$. By denoting $K = \Gamma^{-1}$ and partitioning K in an obvious manner, we have

$$\pi(x_1, x_2) \sim \exp\{-\tfrac{1}{2}(x_1^{\mathrm{T}} K_{11} x_1 + 2x_1^{\mathrm{T}} K_{12} x_2 + x_2^{\mathrm{T}} K_{22} x_2)\}.$$

By completing the term in the exponential to squares with respect to x_2 gives further

$$\pi(x_1, x_2) \sim \exp\{-\tfrac{1}{2}((x_2 + K_{22}^{-1} K_{21} x_1)^{\mathrm{T}} K_{22}(x_2 + K_{22}^{-1} K_{21} x_1) + x_1^{\mathrm{T}}(K_{11} - K_{12} K_{22}^{-1} K_{21}) x_1)\}.$$

By integrating out x_2, we find that

$$\pi(x_1) \sim \exp\{-\tfrac{1}{2} x_1^{\mathrm{T}} \tilde{K}_{22} x_1\},$$

where $\tilde{K}_{22}$ is the Schur complement of K_{22}. However, by the formula (38), the inverse of the Schur complement $\tilde{K}_{22}$ is the first block of the inverse of K, i.e. Γ_{11}. Hence, the marginal covariance of x_1 is Γ_{11} and we have formula (35).

References

[1] Arridge S R 1999 Optical tomography in medical imaging *Inverse Problems* **15** R41–93

[2] Nickell S, Hermann M, Essenpreiss M, Farrell T, Krämer U and Patterson M 2000 Anisotropy of light propagation in human skin *Phys. Med. Biol.* **45** 2873–86

[3] Case M C and Zweifel P F 1967 *Linear Transport Theory* (New York: Addison-Wesley)

[4] Groenhuis R A J, Ferwerda H A and Ten Bosch J J 1983 Scattering and absorption of turbid materials determined from reflection measurements. 1: theory *Appl. Opt.* **22** 2456–62

[5] Schweiger M, Arridge S R, Hiraoka M and Delpy D T 1995 The finite element method for the propagation of light in scattering media: boundary and source conditions *Med. Phys.* **22** 1779–92

[6] Arridge S 2001 Optical tomography *Scattering* ed R Pike and P Sabatier (London: Academic)

[7] Tuch D S, Wedeen V J, Dale A M, George J S and Belliveau J W 1999 Conductivity mapping of biological tissue using diffusion MRI *Ann. NY Acad. Sci.* **888** 314–16

[8] Tarantola A 1987 *Inverse Problem Theory* (Amsterdam: Elsevier)

[9] Kaipio J P, Kolehmainen V, Somersalo E and Vauhkonen M 2000 Statistical inversion and Monte Carlo sampling methods in electrical impedance tomography *Inverse Problems* **16** 1487–522

[10] Järvenpää S 2001 Implementation of PML absorbing boundary condition for solving Maxwell's equations with Whitney elements *PhD Thesis* University of Helsinki

[11] Gilks W R, Richardson S and Spiegelhalter D J 1996 *Markov Chain Monte Carlo in Practice* (London: Chapman and Hall)